Published in final edited form as:
Radiat Res. 2009 February ; 171(2): 236–244. doi:10.1667/RR1470.1.

Nanoscintillator Conjugates as Photodynamic Therapy-Based Radiosensitizers: Calculation of Required Physical Parameters

Nicole Y. Morgan[a,1], **Gabriela Kramer-Marek**[b,c], **Paul D. Smith**[a], **Kevin Camphausen**[b], and **Jacek Capala**[b]

[a]Laboratory of Bioengineering and Physical Science, NIBIB, National Institutes of Health, Bethesda, Maryland 20892 [b]Radiation Oncology Branch, NCI, National Institutes of Health, Bethesda, Maryland 20892 [c]A. Chelkowski Institute of Physics, University of Silesia, Uniwersytecka 4, 40-007 Katowice, Poland

Abstract

The recent demonstration of nanoscale scintillators has led to interest in the combination of radiation and photodynamic therapy. In this model, scintillating nanoparticles conjugated to photosensitizers and molecular targeting agents would enhance the targeting and improve the efficacy of radiotherapy and extend the application of photodynamic therapy to deeply seated tumors. In this study, we calculated the physical parameters required for these nanoparticle conjugates to deliver cytotoxic levels of singlet oxygen at therapeutic radiation doses, drawing on the published literature from several disparate fields. Although uncertainties remain, it appears that the light yield of the nanoscintillators, the efficiency of energy transfer to the photosensitizers, and the cellular uptake of the nano-particles all need to be fairly well optimized to observe a cytotoxic effect. Even so, the efficacy of the combination therapy will likely be restricted to X-ray energies below 300 keV, which limits the application to brachytherapy.

INTRODUCTION

Radiation therapy is an essential tool for the treatment of cancer. Typically, the higher the dose, the more effective the radiotherapy is in eradicating cancer. However, higher radiation doses also lead to more numerous and more severe normal tissue complications, including the risk of serious damage. These complications can be reduced by more precise targeting of the cancer cells using combination therapies. For example, the use of tumor-specific chemical agents such as chemotherapeutic drugs or radiosensitizers can increase killing of the targeted cancer cells without a concomitant increase in the radiation-induced damage to normal cells. Unfortunately, many of the drugs in current clinical use have poor selectivity for tumor cells; thus their toxicity can also produce severe side effects.

Photodynamic therapy (PDT) has been used for many years to treat many diverse human diseases, including macular degeneration, several dermatological disorders, and oncology (1). PDT uses photosensitizers that can be preferentially localized in pathological tissue. The interaction of the photosensitizer and light results in the generation of cytotoxic species, including singlet oxygen ($^1O_2$), free radicals and peroxides, that attack key structural entities within the targeted cells. These very toxic species are characterized by a short lifetime

[1]Address for correspondence: Laboratory of Bioengineering and Physical Sciences, NIBIB, Building 13, Room 3N18, National Institutes of Health, Bethesda MD 20892; morgann@mail.nih.gov.

(<0.04 μs) and a short radius of action. Therefore, the damaged area is essentially confined to tissue that both contains the photosensitizer and is exposed to light.

Relative to current treatments, such as surgery, radiation therapy and chemotherapy, PDT is also comparatively non-invasive, may be more accurately targeted, and is not subject to the total-dose limitations associated with radiotherapy (2). Despite these advantages, PDT has not yet gained general clinical acceptance. The photosensitizers that have been approved for routine PDT treatment absorb light in the visible spectral regions below 700 nm, thus preventing access to more deeply residing tumors. As a result, even with the advent of more sophisticated light delivery systems, the clinical application of PDT is limited to skin lesions, superficial solid tumors, or endoscopically accessible regions. The development of photosensitizers with absorbance in the near-infrared region, which would help overcome the limitation on the penetration depth, is an active area of research. Improving the efficiency of singlet oxygen production in the tissue microenvironment would permit reduction of the concentration of the photosensitizer necessary to treat the tumor. Finally, it would be helpful to develop better molecular targeting to improve the selectivity of the photosensitizers for the diseased tissue. Nano-particles are being investigated as a means to improve the delivery of water-insoluble photosensitizers for conventional photodynamic therapy, and semiconductor quantum dots have been used to directly generate singlet oxygen as well as for exciting attached photosensitizer molecules (3).

The combination of radiotherapy with photodynamic therapy, exploiting the tissue penetration of ionizing X radiation and the cell-level targeting of PDT, might provide a novel approach to overcome the problems with penetration depth and might permit a decrease in the radiation dose without compromising clinical efficacy. It has already been observed that under certain conditions, some photosensitizers act as radiosensitizers, although the molecular mechanism for this effect is not understood. The combination of Photofrin, an FDA-approved photosensitizer, with radiation therapy led to significant enhancements in cytotoxic and apoptotic death of cancer cells (4, 5).

Recently, there has been interest in developing a nano-particle-based photosensitizer delivery system that could combine PDT with radiation therapy. In one model, proposed by Chen *et al.*, the inorganic nanoparticle cores would act as scintillators, which absorb incident X rays and emit visible light (6, 7). Photosensitizer molecules attached to the surface of these nanoscintillators are then activated either by the emitted light or through direct energy transfer, thereby producing toxic amounts of free radicals in any desired location of the body. These nanoparticles would expand the application of PDT to the treatment of deeply located tumors. In addition, it might be possible to conjugate molecules for receptor-mediated internalization to the nanoparticles, ensuring delivery to the intracellular space, and perhaps even targeting vulnerable subcellular structures.

Several doped nanoparticles ($LaF_3:Ce^{3+}$, $LuF_3:Ce^{3+}$, $CaF_2:Mn^{2+}$, $CaF_2:Eu^{2+}$, $BaFBr:Eu^{2+}$) and semiconductor nanoparticles (ZnO, ZnS and TiO_2) have been discussed as potential light sources for use in a nanoparticle-PDT system. The emission spectra of these nanoparticles can be matched perfectly to the absorption spectra of Photofrin®, fullerenes and TiO_2 nanoparticles. For example, $BaFBr:Eu^{2+}:Mn^{2+}$ nanoparticles excited by X rays have three emission bands, peaking at approximately 400, 500 and 640 nm (6). The emission spectrum of these nanoparticles is well matched to the absorption spectrum of hematoporphyrin. Another example is the X-ray luminescence spectrum of $LaF_3:Ce^{3+}$ nanoparticles, with maximum emission at 350 nm, tailing to 500 nm, which matches the absorption spectra of most photosensitizers (6). If successful, this approach could lower the external radiation doses necessary to control cancer and thereby minimize the side effects while enhancing the benefits of radiation therapy.

The aim of the present review is to estimate the amount of light that can be produced by nanoscintillators, including those proposed by Chen *et al.*, in response to radiation doses typically used in radiotherapy, and to assess the consequent activation of the attached photosensitizer as well as the theoretical effectiveness of the produced free radicals. Our results set the requirements that may guide further development of this innovative new application of nanotechnology and PDT.

GENERAL APPROACH

In this paper, we draw on recent literature, combining results for nanoparticle targeting of tumor tissue, focusing on the systemic delivery of molecularly targeted nanoparticles, and singlet oxygen measurements in PDT. From these experimental results, we are able to better establish the physical parameters required for nanoparticles to be effective either in X-ray-stimulated PDT or as radiosensitizers. We have obtained best-guess estimates for the likely amount of cellular uptake of nanoparticles, the amount of radiation absorbed by the nanoparticles relative to the dose delivered to the tissue, and the limits on the light yield and singlet oxygen generation efficiency of the nanoparticle conjugates. From these parameters, we can calculate the amount of singlet oxygen generated in tissue as a function of X-ray energy and dose and compare these numbers with literature values for the killing dose of singlet oxygen found in PDT experiments. These are prospective estimates; to our knowledge, nanoparticles that are well suited for this purpose have not yet been made. The intent of this work is to stimulate discussion and to help direct synthesis efforts toward materials and experiments with the best possible chance of success.

For simplicity in comparing different results, in these calculations we will assume a spherical cell 10 μm diameter, of density 1 g/ml, and calculate the number of singlet oxygen molecules generated per cell, N_{1O_2}. The amount of singlet oxygen generated per cell by these nanoparticle-photosensitizer conjugates is given by

$$N_{1O_2} = 3.2D \times Mv \times \Phi_{1O_2}, \quad (1)$$

where D is the X-ray dose in Gy delivered to the surrounding tissue; M (unitless) is the absorption of the nanoparticle cores relative to that of tissue and is strongly dependent on incident X-ray energy; v is the volume fraction of the cell occupied by the nanoparticle cores, also unitless. Φ_{1O_2} denotes the efficiency with which incident X-ray energy is converted into singlet oxygen, in units of molecules of singlet oxygen generated per MeV absorbed X rays. The conversion factor 3.2 arises from the conversion between Gy and MeV: 1 Gy delivered to a 10-μm-diameter cell corresponds to an absorbed energy of $(6.2 \times 10^{12}$ MeV/J$)(5.2 \times 10^{-13}$ kg) = 3.2 MeV. In the following sections, we use published results from a number of different fields to obtain estimates for these parameters to calculate N_{1O_2}.

NANOPARTICLE LOADING

There are a number of medical applications for nanoparticles, ranging from their use as contrast agents to the delivery of therapeutics, some of which have progressed to commercial products (8–11). For almost all of these applications, the nanoparticles must be delivered to specifically targeted cells and must be taken up efficiently by those cells. This is partly a size constraint and partly will be determined by molecular targeting by ligands attached to the nanoparticle surface.

To estimate the maximum loading of nanoparticles into tumor tissue, we turn to literature reports on the cellular uptake of functionalized nanoparticles. Although there have been

extensive studies of nanoparticle uptake by cells and tissues, relatively few of these papers provide quantitative estimates for the amount of material taken into the tissue. Furthermore, most of the studies that do provide quantification focus on relative changes in uptake as a result of receptor targeting, etc., as opposed to the typical or maximum possible loading of cells. A representative sampling of published results is presented in Table 1. In calculating the volume fraction occupied by the nanoparticles, we have assumed a 10-μm-diameter spherical cell that has a volume of 0.52 pl, for simplicity. In fact, cancer cells are often somewhat larger, with reported volumes of 1–1.8 pl for *in vitro* measurements, depending on the cell line (12).

In general, the reported cellular uptake of iron oxide nanoparticles is much higher than that of gold nanoparticles or semiconductor quantum dots (Table 1). This is likely due to variations in experimental protocol, or possibly because the iron oxide nanoparticles are more likely candidates for biology laboratories due to their greater availability, including the clinical approval of dextran-coated nanoparticles (e.g., Feridex). In addition, there are a number of straightforward assays available for quantification of iron content in cells, whereas the techniques for quantifying cell loading with gold or semiconductor nanoparticles are more limited.

The published numbers for iron oxide particles show considerable variation, but the variations are roughly consistent with what might be expected given the differences in experimental parameters. We assume that the capping molecules are broken down over the course of the experiment, so that only the core volume is the important parameter; if this is not the case, some of these results correspond to a volume fraction greater than unity. This is a significant simplification, because the extent to which the encapsulating shell is broken down will depend on the composition of the shell, the degree of crosslinking, and the incubation time.

Two papers, by Lewin *et al.* and Frank *et al.*, report loading of roughly 30 pg of iron per cell, which corresponds to a volume fraction of 1.6%, using similar incubation times (1 and 2 h) and similar iron concentrations in the cell medium (40 and 25 μg/ml, respectively) (13, 14). Another paper, by Weissleder *et al.*, gets a much lower iron concentration, roughly 1 pg iron per cell in a pancreatic cancer line (PaCa-2), using 3 nm monocrystalline iron oxide particles with crosslinked dextran shells and a 4-h incubation period with 1 mg/ml iron (15). If we consider only the nanoparticle core, this corresponds to a 0.05% volume fraction; however, if the dextran shell is broken down more slowly in the cell because of the crosslinking, then we should use something closer to the 38-nm total particle diameter. This corresponds to a volume fraction of slightly more than one.

Other groups report substantially higher loading. Zhang *et al.* reported achieving 113 pg of iron per cell, using PEG-coated magnetite particles at a concentration of 200 μg/ml iron and a 4-day incubation period; this corresponds to a 6% volume fraction, again counting only the core volume, as measured with induction-coupled plasma emission spectroscopy (16). A later paper by the same authors reports a concentration of approximately 650 pg of iron per cell for nanoparticles with PEG-folic acid, corresponding to a volume fraction of 33.7% (17). Leuschner *et al.* also reported a very high iron concentration, measured with Prussian blue, of 453 pg of iron per cell, after 1 h incubation with luteinizing hormone releasing hormone (LHRH)-functionalized nanoparticles at a concentration of 7.6 mg/ml iron (18). This corresponds to a volume fraction of 23.5%. It is possible that our rough calculations significantly overstate the volume fraction for these last two results; in particular, for these *in vitro* experiments, it seems likely that the cell volume could change with the nanoparticle uptake, particularly at these high loading fractions. Alternately, it may be possible that the cell is larger than 10 μm or that some nanoparticles adhere to the outside of the cells even

after the washing protocols. However, if the particles are being used as radio- or photosensitizers, it may not be important whether the nanoparticles are inside or immediately outside the cell.

Of particular relevance to this application, Leuschner *et al.* also performed an *in vivo* experiment, in which mice infected with MDA-MB-435S.luc cells, a human breast cancer line transfected with the luciferase gene, are given a tail vein injection of LHRH nanoparticles at a dose of 250 mg/kg (18). After 20 h, 60% of the injected dose was found to accumulate at the primary tumor. Furthermore, by using the luciferase reaction to quantify the number of metastatic cells in homogenized lung tissue, the researchers were able to estimate that these cells accumulated nano-particles at a concentration of roughly 80 pg iron per cell, corresponding to a volume fraction of 4% iron oxide in the metastatic cells.

The published numbers for cellular uptake of gold nano-particles are substantially lower, although this may be due to differences in incubation conditions; in general, lower nanoparticle concentrations are used during incubation. Chithrani *et al.* studied citric acid-stabilized gold nanoparticles of varying sizes and shapes and found maximum uptake corresponding roughly to a 0.1% volume fraction (19). However, the cells were incubated with 15 μg/ml gold nanoparticles compared to 7.6 mg/ml iron for the iron-particle experiments of Leuschner *et al.* Similarly, Dixit *et al.* studied gold nanoparticles functionalized with PEG and folic acid, similar to the iron oxide particles of Zhang *et al.*, but the maximum volume fraction they obtained was 0.05%, as measured by TEM of cryoslices. In this case, the cells were incubated with 5×10^{11} nanoparticles per milliliter, or roughly 5 μg/ml gold. As far as we know, no one has tried transfection of cells under the same conditions as with iron oxide nanoparticles, but it is also possible that there is clustering of the protein-coated SPION particles that increases loading of the cells.

To sum up, we will rely on the experiments with iron nanoparticles, primarily the *in vitro* experiments of Frank and Lewin, as well as the *in vivo* experiment of Leuschner, and take a 5% volume fraction for the nanoparticle cores as a potentially difficult but attainable goal. One factor that may act in our favor is that it is not essential that all the particles in the tumor tissue be taken up by the cells, as long as they are sufficiently close for the singlet oxygen to attack the cell membranes. Alternatives to systemic delivery, such as direct injection of nanoparticles into a tumor mass, could also result in a higher volume fraction of nano-particles.

RADIATION ABSORBED BY NANOPARTICLES

The major question in considering the use of nanoparticle PDT for enhancing radiotherapy is what level of effect we expect to see at therapeutic radiation doses. For radiotherapy, the most common fractionation schedule is for daily fractions of 2 Gy, to a total radiation dose of 50–70 Gy, with a typical energy of 6–20 MeV for an external source. In contrast, brachytherapy provides a continuous dose of lower-energy radiation from implanted sources; typical doses are of the order of 65 Gy delivered over 5–6 days, at energies of 27–35 keV (^{125}I, γ rays), through 300–610 keV (^{192}Ir, γ rays), 410–1009 keV (^{198}Au, γ rays), and 190–2430 (^{226}Ra, γ rays).

Using published values for atomic mass attenuation coefficients, we can calculate how much radiation will be absorbed by the nanoparticles relative to the tissue. For example, LaF_3, a lanthanide scintillator, has a density of 6.1 g/cm^3; using the atomic masses of lanthanum and fluorine, the compound is 70.9% lanthanum and 29.1% fluorine by weight. The amount of radiation absorbed by the LaF_3 nanoparticles relative to an equal volume of tissue is then given by

$$M = \frac{\rho_{LaF_3}}{\rho_t} \times \frac{(0.709 \times \mu_{La}) + (0.291 \times \mu_F)}{\mu_t}, \quad (2)$$

where ρ_{LaF3} and ρ_t are the densities of the nanoparticle core and the surrounding tissue, and μ_{La}, μ_F and μ_t are mass energy absorption coefficients for the respective elements and for soft tissue, obtained from the NIST database (20). The values for the mass energy absorption coefficients depend strongly on the X-ray energy. In Fig. 1 we plot calculations for the relative absorption for two lanthanide scintillators, LaF_3 and LuI_3, as a function of X-ray energy. LaF_3 was chosen because a synthetic route for LaF_3 nanoparticles has already been developed, and LuI_3 was chosen because bulk cerium-doped LuI_3 has the highest reported light yield for this class of materials, 10^5 photons/MeV absorbed energy (21, 22). However, the method here is easily extended to any proposed nanoscintillator material. The plotted curves show the relative absorption of the scintillators compared to an equal volume of soft tissue.

The data in Fig. 1 ignore the effect from dopant atoms, because the dopant concentration is often varied. In nano-particles, the dopant concentration can be particularly hard to define, because the dopant atoms may segregate near the surface. Including the dopant properties would not cause large changes away from the absorption edges of the atoms for small to moderate dopant concentrations.

The absorption of the nanoparticles is substantially greater at lower X-ray energies. Above 300 keV, the absorption of the nanoparticles is less than 20 times that of an equal volume of soft tissue; if the nanoparticles occupy no more than a 5% volume fraction, the X-ray absorption by the surrounding tissue will be greater than that of the nanoparticles. Although it would still be possible to investigate the use of the nanoparticles as radiosensitizers at these energies, focusing on X-ray energies approximately 300 keV or below gives a substantially greater chance of success. At these energies, there will be significant local attenuation of radiation. This is most likely not a problem for implants, because the attenuation lengths ($1/e$) for 30 keV photons are roughly 220 μm for LaF_3 and 3 cm for tissue. Since the nanoparticles are ~50 nm in diameter, the attenuation in LaF_3 will be negligible unless the density is very high.

SINGLET OXYGEN GENERATION EFFICIENCY

The proposed mechanism for enhancement of PDT by nanoparticle scintillators is through energy transfer between the nanoparticle cores and the conjugated photosensitizers, followed by singlet oxygen generation by the photosensitizers. Although there are other cytotoxic species generated by excitation of photosensitizers, singlet oxygen is the most common and is efficiently generated in non-hypoxic tissue. The efficiency of singlet oxygen generation can be approximated by

$$\Phi_{^1O_2} = \varphi_s \times \varphi_{FRET} \times \varphi_p, \quad (3)$$

where ϕ_s is the light yield of the nanoparticle scintillator, given in units of photons generated per MeV of absorbed X-ray energy. ϕ_{FRET} is the efficiency of the energy transfer from the scintillator core to the conjugated photosensitizer, and ϕ_p is the efficiency with which the excited photosensitizer generates singlet oxygen; both of these quantities range between zero and one.

We will assume that the nanoparticle conjugates can be engineered such that $\phi_{FRET} \geq 0.75$ and $\phi_p \geq 0.89$, using literature values for related systems. The value of ϕ_p for a particular photosensitizer depends greatly on the environment, and particularly on whether the photosensitizer molecules form oligomers or aggregates. It seems likely that aggregate formation could be less of a problem if the photosensitizer molecules are conjugated to nanoparticles. For our calculations, we will use $\phi_p = 0.89$, as measured by Fernandez *et al.* for Photofrin® in oxygen-saturated 10 m*M* pH 7.4 phosphate buffer with 1% Triton X-100 and excited with green light (23). This number is perhaps overly optimistic: $\phi_p = 0.89$ is substantially higher than has been measured for Photofrin® under different solution conditions (24). Furthermore, the oxygen concentration in tissue (pO_2 ~5%) is lower, which might lead to lower production of singlet oxygen in tissue, although this effect is difficult to quantify (M. Cherikuri, private communication). However, the concept of nanoscintillator-photosensitizer conjugates is not limited to Photofrin®, and it appears that achieving $\phi_p \sim 0.9$ with new compounds might be feasible (25).

The quantum dot FRET biosensors from Medintz *et al.* have $\phi_{FRET} = 0.75$ for energy transfer from the quantum dot cores to maltose-binding protein-Cy3 complexes conjugated to the nanoparticle surface (26). Although the FRET efficiency for transfer between the nanoparticle and a single conjugated molecule was only about 0.15, each nanoparticle core was conjugated to 10 protein molecules, substantially raising the overall efficiency. However, we note that FRET efficiency is a strong function of distance and is highest for a 20–60-Å separation between donor and acceptor. In the biosensors of Medintz *et al.*, this distance is approximately 68 Å, for a quantum dot radius of ~30 Å; the donor position is the center of the quantum dot, and the acceptor is the location of the dye bound to the protein on the QD surface. Keeping this distance below ~75 Å for the nanoscintillators could place strong restrictions on the size of the nanoparticle core and the conjugation chemistry used to attach the photosensitizers.

One of the aims of this paper is to estimate the value of the light yield ϕ_s required for the nanoparticles to be effective as PDT agents or as radiosensitizers. However, we can establish some boundaries from the literature and from basic physics. As far as we know, the highest reported light yield for a bulk lanthanide compound is 10^5 photons per MeV absorbed energy for LuI_3:Ce (21, 22). However, for this material, the emitted light falls in a range of wavelengths; for our purposes, this would mean that some fraction, perhaps half, of the emitted light might not be efficient at exciting the conjugated porphyrins. If we consider the emission of 480 nm light (2.58 eV per photon), the absolute theoretical maximum, i.e., perfect energy conversion, gives 3.9×10^5 photons/MeV. For longer wavelengths this is a little better: At 660 nm, perfect energy conversion corresponds to 5.4×10^5 photons/MeV. Although it is possible that nanoscintillators might have some advantage over the bulk materials, in our judgment they are unlikely to have substantially better than 50% of this perfect conversion efficiency.

Using these estimates, which assume nearly perfect optimization of the nanoparticle parameters, we can calculate the number of singlet oxygen molecules generated per cell for an X-ray dose of 60 Gy as a function of energy. The result is shown in Fig. 2. For the light yield, we have assumed 50% energy conversion for 660 nm light, which corresponds to 2.7×10^5 photons/MeV. The horizontal line is the estimated killing dose (reduction of cell population to 1/*e*) of singlet oxygen taken from Niedre *et al.* (27); this number is an order of magnitude estimate and is by far the lowest in the literature, as discussed in the next section.

COMPARISON TO KILLING DOSE

In determining the light dose needed for successful photodynamic therapy, there are a number of parameters that can be difficult to measure directly. The concentration of the photosensitizer in tissue, the oxygenation of the tissue, and the penetration of the excitation light to the photosensitizer all directly affect the light dose required for a cytotoxic effect. Recently, the development of more sensitive NIR detectors has permitted the development of singlet oxygen luminescence dosimetry (SOLD), in which the 1270-nm emission of singlet oxygen is measured directly *in vitro* or *in vivo.* To simplify our discussion of the nanoparticle scintillators, we focus on the dose estimates obtained from this method. Niedre *et al.* estimate that 5.6×10^7 molecules of $^1O_2$ are needed to kill a cell of similar size as above, based on *in vitro* measurements of OCI-AML5 leukemia cells (reduction of cell population to 1/*e* fraction) (27). Because the experiments were done in culture, the environment was oxygen-rich and the attenuation of light in the samples was minimal. Other estimates are substantially higher, including a later paper by the same group, which estimated that 5.8×10^{10} molecules of $^1O_2$ are needed to kill normal mouse epidermal cells *in vivo* (ALA-PpIX) (28), assuming a cell volume of 1 pl. These numbers also track published estimates for singlet oxygen dose as measured through photobleaching of the photosensitizers, ranging from 2×10^8 molecules to 7×10^9 molecules of singlet oxygen per cell (29–31). The subcellular location of singlet oxygen generation may affect the cytotoxicity, and it is not well controlled for these experiments. Also, the Niedre calculations include estimates of the light collection efficiency of the experimental apparatus as well as of the probability of radiative decay of the singlet oxygen in tissue; the resulting calculation could be considered an order-of-magnitude estimate.

In Fig. 3 we use the smallest number for the killing dose (5.6×10^7 molecules per cell) to calculate the required light yield for these nanoscintillators to have a PDT effect at therapeutic radiation doses. The calculation assumes a radiation dose of 60 Gy, $\phi_{FRET} = 0.75$, and $\phi_p = 0.89$ and assumes that the nanoparticle cores occupy a 5% volume fraction in the tissue. To provide an indication of when a radiosensitizing effect from the nanoparticles might be observed, a line corresponding to a tenth of the killing dose, or 5.6×10^6 $^1O_2$ molecules per 10-μm-diameter cell, has been included. Although the singlet oxygen concentration in this case falls below the reported cytotoxic level, cells already damaged by radiation therapy may be affected. Reference lines indicating reasonable ceilings for expected light yield are also plotted.

DISCUSSION

These calculations can be easily applied to new candidate materials and nanoconjugates to estimate whether a PDT or radiosensitizing effect is likely to be observed. As an example, in Fig. 4 we have used Eq. (1) to calculate the number of singlet oxygen molecules generated per cell as a function of X-ray dose for several different X-ray energies and compared these numbers to the killing dose of singlet oxygen from Niedre (27). It is clear from this and the other figures that there is likely to be a substantially larger cytotoxic effect for X-ray energies below ~200 keV, which would likely restrict the use of these particles to brachytherapy, and that the largest effect is expected for X-ray energies around 50 keV. It is possible that these numbers will shift slightly if other materials are used for the nanoscintillator cores; this effect can be calculated for a candidate material by adjusting Eq. (2) accordingly.

As a simple example, applying Eq. (2) to gold nanoparticles gives a relative absorption four to five times higher than for the nanoscintillators described here, with a similar dependence on X-ray energy. Monte Carlo simulations of radiation dose enhancement by gold

nanoparticles as a function of the tumor position in tissue for several clinically relevant cases also showed a clear preference for sub-MeV X-ray energies (32). Theoretically, the irradiation of high-*Z* elements such as gold at their K-edge absorption energy leads to emission of Auger electrons and photoelectrons, releasing a large amount of energy with nanoscale localization, which results in enhanced damage to nearby cells and even subcellular structures (33). Gold nanoparticles have already been used successfully in combination with radiotherapy on tumor-bearing mice: Hainfeld *et al.* used 250 kVp X rays with 1.9-nm gold nanoparticles and found a 1-year survival rate of 86% for animals treated with the combination therapy compared to 20% with X rays alone and 0% with gold alone (34). The much greater relative absorption of gold at X-ray energies in the 50–200 keV range suggests that brachytherapy could be a fruitful approach for combination therapies with gold nanoparticles as well, although with extremely high dose enhancement, it might be possible to use external radiation sources at doses low enough that skin damage would be avoided. It is possible that gold nanoparticles might also present a plausible alternative to nanoscintillators for combining radiotherapy and PDT if the energy released by gold after X irradiation could activate photosensitizers, but the analysis of this proposition is beyond the scope of the present work.

In looking at the estimates in Fig. 4 for the nanoscintillator-photosensitizer conjugates, we expect cytotoxicity at substantially sublethal radiation doses only for X-ray energies in the 30–100 keV range, assuming that both the nanoscintillators and their conjugation to photosensitizers are well optimized and that the low estimate for the $^1O_2$ killing dose is correct. It seems more likely that these particles could first find clinical application as radiosensitizers, improving the efficacy of radiotherapy. Alternately, one could imagine mechanisms by which the nanoparticles, upon activation by X radiation, trigger therapeutic cascades, perhaps by releasing therapeutic agents such as drugs, or biological response modifiers, including genetic material. In this case, singlet oxygen generated by these conjugates could easily have a cytotoxic effect on already-weakened cells, at levels well below those found in experiments that only used PDT. In addition, the hypoxia typical in solid tumors is one of the limiting factors in PDT, in that the oxygen concentration can be too low for the efficient generation of singlet oxygen by the photosensitizers. If there were some method to engineer a nanoparticle coating that could break down upon irradiation, increasing the local oxygen concentration just as the energy to generate singlet oxygen was also present, this might also improve the prospects for PDT of deep-seated tumors.

Recently, there has been considerable research on the development of new photosensitizers with high quantum yield, longer wavelength excitation, and better resistance to photobleaching. Although these compounds would clearly be of great interest for conventional PDT, for these calculations we have already assumed a singlet oxygen generation quantum yield of $\phi_p = 0.89$ and also that the nanoparticle emission spectrum could be well matched to existing photosensitizers. In addition, for this modality it seems likely that radiation dose rather than photodegradation of the conjugated photosensitizer will be the limiting factor.

There remain a number of uncertainties in this system, and the estimates above should be considered order-of-magnitude calculations. Some of the uncertainty arises from the large variations in the reported values for physical parameters such as cellular uptake and the singlet oxygen killing dose, as discussed above. In choosing values for these estimates, we have deliberately chosen values that are optimistic but that could be attainable physically. Although the text focused on systemic injection with molecular targeting for nanoparticle delivery, direct injection of nano-particles into tumor tissue could achieve concentrations in excess of the 5% volume fraction used in the calculations above. A more complicated question is whether and how the time scale for delivery of singlet oxygen affects the dose

required for cell death. Niedre *et al*. found that cell death corresponds directly to the cumulative amount of singlet oxygen generated, independent of treatment time, for conventional PDT lasting up to 60 min (27). However, for implanted radiation sources used in combination with the nanoscintillator conjugates, the cells will likely be exposed to a lower level of insult for a substantially longer time.

CONCLUSION

There is excitement over the prospect of tailoring nano-particles for novel therapies, such as the combination of radiation and photodynamic therapy discussed here. For these new proposed applications, it is helpful to combine information from the literature and physical principles to obtain quantitative estimates for the expected efficacy under a range of physical parameters. In this case, a review of the scientific literature in several disparate fields led to estimates that suggest these nanoparticle-photosensitizer conjugates are more likely to be useful when irradiated with X-ray energies below a few hundred keV. In addition, we have established a straightforward calculation for evaluating new candidate materials; hopefully these results will assist in directing efforts to synthesize nanoparticles for this application.

Acknowledgments

This research was supported by the Intramural Research Program of the National Institutes of Health, National Cancer Institute, and National Institute of Biomedical Imaging and Bioengineering. The authors thank Murali Cherukuri and Wei Chen for helpful discussions.

References

1. Palumbo G. Photodynamic therapy and cancer: a brief sightseeing tour. Expert Opin Drug Deliv. 2007; 4:131–148. [PubMed: 17335411]
2. Brown SB, Brown EA, Walker I. The present and future role of photodynamic therapy in cancer treatment. Lancet Oncol. 2004; 5:497–508. [PubMed: 15288239]
3. Samia ACS, Dayal S, Burda C. Quantum dot-based energy transfer: Perspectives and potential for applications in photodynamic therapy. Photochem Photobiol. 2006; 82:617–625. [PubMed: 16475871]
4. Schaffer M, Ertl-Wagner B, Schaffer PM, Kulka U, Jori G, Duhmke E, Hofstetter A. The application of Photofrin II (R) as a sensitizing agent for ionizing radiation—A new approach in tumor therapy? Curr Med Chem. 2005; 12:1209–1215. [PubMed: 15892632]
5. Kulka U, Schaffer M, Siefert A, Schaffer PM, Olsner A, Kasseb K, Hofstetter A, Duhmke E, Jori G. Photofrin as a radiosensitizer in an *in vitro* cell survival assay. Biochem Biophys Res Commun. 2003; 311:98–103. [PubMed: 14575700]
6. Chen W, Zhang J. Using nanoparticles to enable simultaneous radiation and photodynamic therapies for cancer treatment. J Nanosci Nanotechnol. 2006; 6:1159–1166. [PubMed: 16736782]
7. Liu Y, Chen W, Wang S, Joly AG. Investigation of water-soluble x-ray luminescence nanoparticles for photodynamic activation. Appl Phys Lett. 2008; 92:043901.
8. Wang YXJ, Hussain SM, Krestin GP. Superparamagnetic iron oxide contrast agents: physicochemical characteristics and applications in MR imaging. Eur Radiol. 2001; 11:2319–2331. [PubMed: 11702180]
9. Moghimi SM, Hunter AC, Murray JC. Nanomedicine: current status and future prospects. FASEB J. 2005; 19:311–330. [PubMed: 15746175]
10. Michalet X, Pinaud FF, Bentolila LA, Tsay JM, Doose S, Li JJ, Sundaresan G, Wu AM, Gambhir SS, Weiss S. Quantum dots for live cells, *in vivo* imaging, and diagnostics. Science. 2005; 307:538–544. [PubMed: 15681376]
11. Napier ME, Desimone JM. Nanoparticle drug delivery platform. Polymer Rev. 2007; 47:321–327.

12. Pilatus U, Shim H, Artemov D, Davis D, vanZijl PCM, Glickson JD. Intracellular volume and apparent diffusion constants of perfused cancer cell cultures, as measured by NMR. Magn Reson Med. 1997; 37:825–832. [PubMed: 9178232]
13. Lewin M, Carlesso N, Tung CH, Tang XW, Cory D, Scadden DT, Weissleder R. Tat peptide-derivatized magnetic nano-particles allow *in vivo* tracking and recovery of progenitor cells. Nat Biotechnol. 2000; 18:410–414. [PubMed: 10748521]
14. Frank JA, Miller BR, Arbab AS, Zywicke HA, Jordan EK, Lewis BK, Bryant LH, Bulte JWM. Clinically applicable labeling of mammalian and stem cells by combining superparamagnetic iron oxides and transfection agents. Radiology. 2003; 228:480–487. [PubMed: 12819345]
15. Weissleder R, Kelly K, Sun EY, Shtatland T, Josephson L. Cell-specific targeting of nanoparticles by multivalent attachment of small molecules. Nat Biotechnol. 2005; 23:1418–1423. [PubMed: 16244656]
16. Zhang Y, Kohler N, Zhang MQ. Surface modification of superparamagnetic magnetite nanoparticles and their intracellular uptake. Biomaterials. 2002; 23:1553–1561. [PubMed: 11922461]
17. Zhang Y, Sun C, Kohler N, Zhang MQ. Self-assembled coatings on individual monodisperse magnetite nanoparticles for efficient intracellular uptake. Biomed Microdevices. 2004; 6:33–40. [PubMed: 15307442]
18. Leuschner C, Kumar CS, Hansel W, Soboyejo W, Zhou J, Hormes J. LHRH-conjugated magnetic iron oxide nanoparticles for detection of breast cancer metastases. Breast Cancer Res Treat. 2006; 99:163–176. [PubMed: 16752077]
19. Chithrani BD, Chan WCW. Elucidating the mechanism of cellular uptake and removal of protein-coated gold nanoparticles of different sizes and shapes. Nano Lett. 2007; 7:1542–1550. [PubMed: 17465586]
20. Hubbell, JH.; Seltzer, SM. Tables of X-Ray Mass Attenuation Coefficients and Mass Energy-Absorption Coefficients; NIST Standard Reference Database. 1996. p. 126http://physics.nist.gov/PhysRefData/XrayMassCoef/cover.html
21. Birowosuto MD, Dorenbos P, van Eijk CWE, Kramer KW, Gudel HU. High-light-output scintillator for photodiode readout: LuI3:Ce^{3+} J Appl Phys. 2006; 99:3520.
22. Kramer KW, Dorenbos P, Gudel HU, van Eijk CWE. Development and characterization of highly efficient new cerium doped rare earth halide scintillator materials. J Mater Chem. 2006; 16:2773–2780.
23. Fernandez JM, Bilgin MD, Grossweiner LI. Singlet oxygen generation by photodynamic agents. J Photochem Photobiol B. 1997; 37:131–140.
24. Wilkinson F, Helman WP, Ross AB. Quantum yields for the photosensitized formation of the lowest electronically excited singlet-state of molecular-oxygen in solution. J Phys Chem Ref Data. 1993; 22:113–262.
25. Pineiro M, Pereira MM, Gonsalves A, Arnaut LG, Formosinho SJ. Singlet oxygen quantum yields from halogenated chlorins: potential new photodynamic therapy agents. J Photochem Photobiol A. 2001; 138:147–157.
26. Medintz IL, Clapp AR, Mattoussi H, Goldman ER, Fisher B, Mauro JM. Self-assembled nanoscale biosensors based on quantum dot FRET donors. Nat Mater. 2003; 2:630–638. [PubMed: 12942071]
27. Niedre MJ, Secord AJ, Patterson MS, Wilson BC. *In vitro* tests of the validity of singlet oxygen luminescence measurements as a dose metric in photodynamic therapy. Cancer Res. 2003; 63:7986–7994. [PubMed: 14633731]
28. Niedre MJ, Yu CS, Patterson MS, Wilson BC. Singlet oxygen luminescence as an *in vivo* photodynamic therapy dose metric: validation in normal mouse skin with topical amino-levulinic acid. Br J Cancer. 2005; 92:298–304. [PubMed: 15655542]
29. Dysart JS, Patterson MS. Characterization of Photofrin photobleaching for singlet oxygen dose estimation during photodynamic therapy of MLL cells *in vitro*. Phys Med Biol. 2005; 50:2597–2616. [PubMed: 15901957]

30. Dysart JS, Singh G, Patterson MS. Calculation of singlet oxygen dose from photosensitizer fluorescence and photobleaching during mTHPC photodynamic therapy of MLL cells. Photochem Photobiol. 2005; 81:196–205. [PubMed: 15469385]

31. Georgakoudi I, Nichols MG, Foster TH. The mechanism of Photofrin(R) photobleaching and its consequences for photodynamic dosimetry. Photochem Photobiol. 1997; 65:135–144. [PubMed: 9066293]

32. Cho SH. Estimation of tumour dose enhancement due to gold nano-particles during typical radiation treatments: a preliminary Monte Carlo study. Phys Med Biol. 2005; 50:N163–N173. [PubMed: 16030374]

33. Carter JD, Cheng NN, Qu YQ, Suarez GD, Guo T. Nanoscale energy deposition by x-ray absorbing nanostructures. J Phys Chem B. 2007; 111:11622–11625. [PubMed: 17854220]

34. Hainfeld JF, Slatkin DN, Smilowitz HM. The use of gold nanoparticles to enhance radiotherapy in mice. Phys Med Biol. 2004; 49:N309–N315. [PubMed: 15509078]

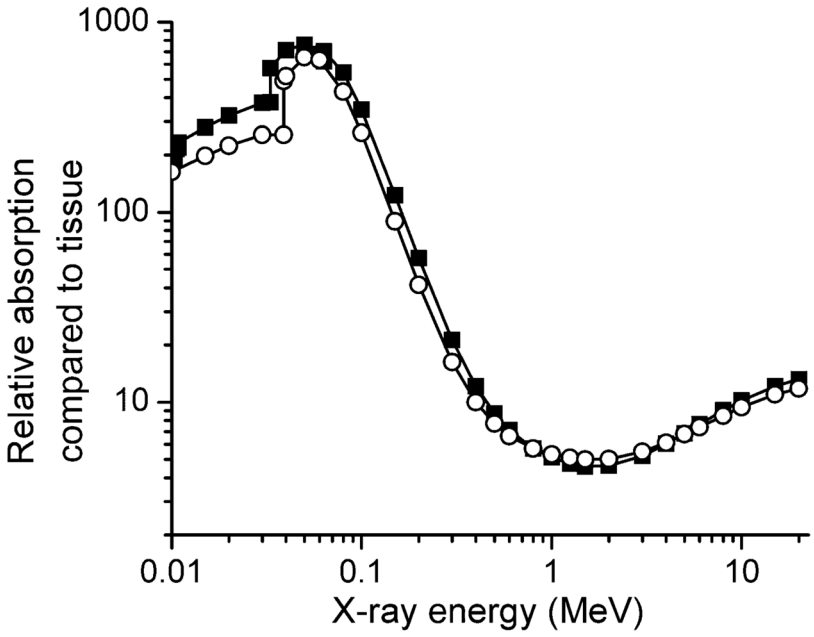

FIG. 1.

The absorption of nanoparticle cores relative to an equal volume of soft tissue for LuI_3 (■) and LaF_3 (○). Absorption coefficients for atomic elements and soft tissue taken from ref. (20).

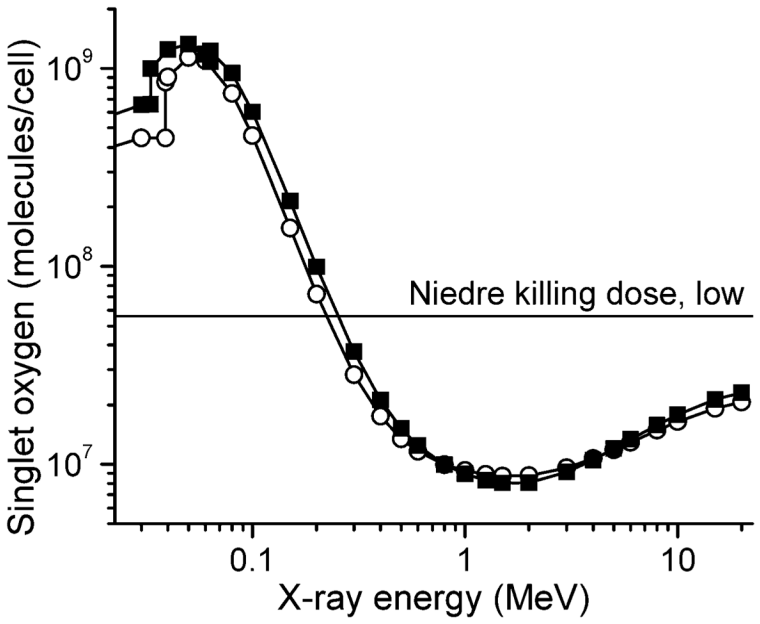

FIG. 2.

The number of singlet oxygen molecules generated in a 10-μm-diameter cell as a function of X-ray energy at a dose of 60 Gy, assuming that the nanoparticle cores occupy 5% of the cell volume, and optimization of the singlet oxygen generation efficiency: ϕ_s = ½ (5.4×10^5 photons/MeV), ϕ_{FRET} = 0.75, and ϕ_p = 0.89. Closed squares: LuI_3; open circles: LaF_3.

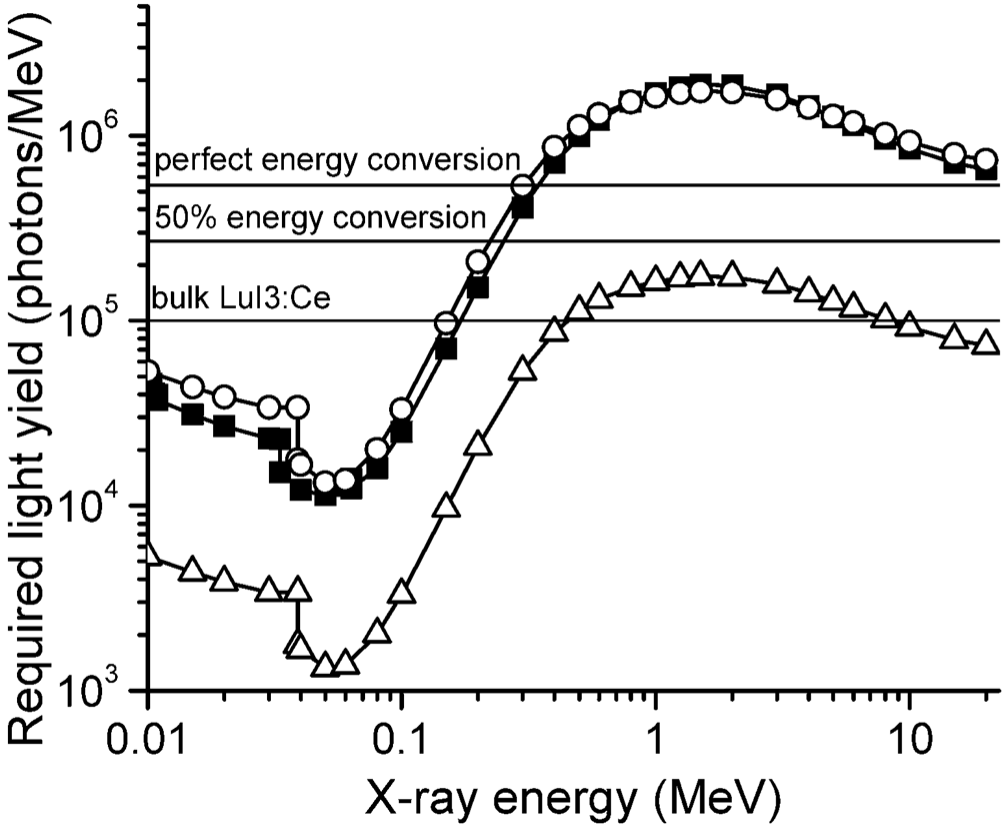

FIG. 3.

The required light yield for nanoscintillators, assuming a 5% volume fraction, $\phi_{FRET} = 0.75$ and $\phi_p = 0.89$, for the full killing dose and 1/10 of the killing dose of $^1O_2$, as discussed in the text. This assumes the low Niedre number (5.6×10^7) for the killing dose; other literature values are one to three orders of magnitude higher. Closed squares: LuI_3, full killing dose; open circles: LaF_3, full killing dose; open triangles: LaF_3, 1/10 killing dose. Horizontal lines indicate literature value for bulk LuI_3:Ce (21) and calculated values for 100% and 50% efficient conversion of absorbed energy into 660 nm light.

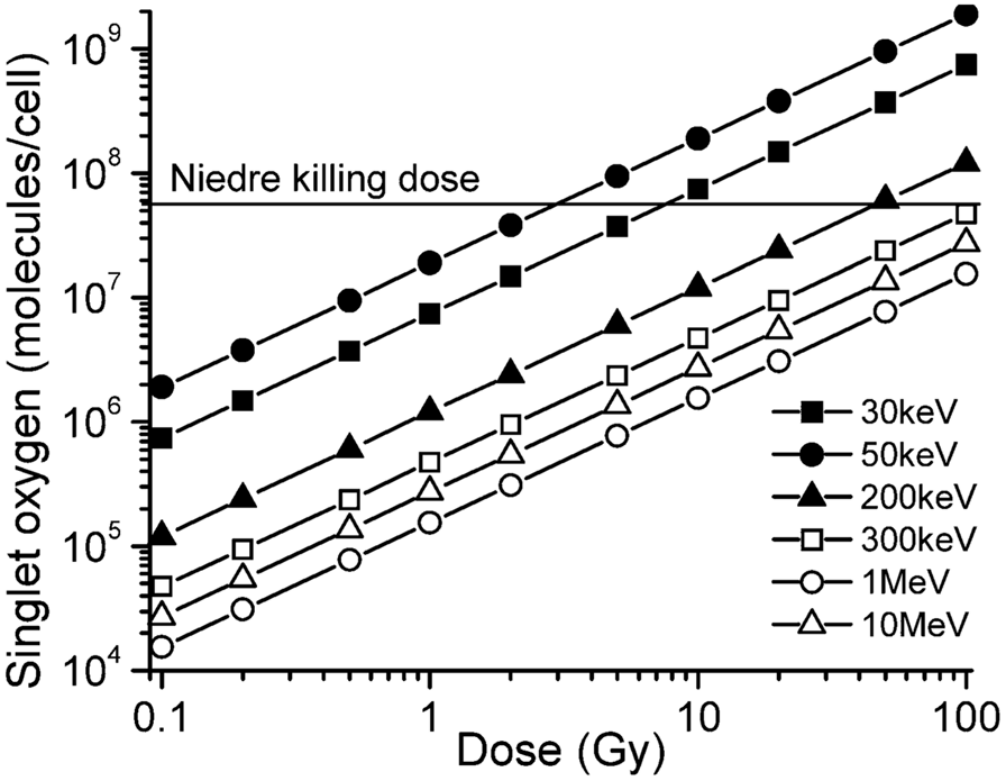

FIG. 4.

The number of singlet oxygen molecules generated per 10-μm-diameter cell as a function of X-ray dose for several different X-ray energies. All lines that assume 5% of volume fraction is occupied with LaF_3 nanoparticles, 50% conversion of X-ray energy into 660 nm photons by nanoparticles, and (0.75 × 0.89) efficiency for conversion of "emitted" photons to singlet oxygen. Horizontal line corresponds to low Niedre number (5.6×10^7) for the killing dose.

TABLE 1

Compilation of Literature Data on Cellular Uptake of Nanoparticles

Material	Core/core-shell diameter (nm)	Incubation conditions	Stated maximum loading[a]	Corresponding volume fraction, core only	Method	Ref.
Feridex/TAs	4.8–5.6/80–150	2 h, 37°C, 25 μg/ml iron	30	1.6%	Ferrozine/MR	(14)
MION/small molecule	3/38	4 h, 37°C, 0.1 mg/ml iron	2.2	0.12%	FITC immunoassay	(15)
^{111}In-labeled CLIO/Tat peptide	5/45	1 h, 37°C, 40 μg/ml iron	30	1.6%	Gamma-ray counter	(13)
Magnetite (Fe_3O_4)/LHRH	10/?	1 h, 37°C, 7.6 mg/ml iron	453	23.5%	Prussian Blue	(18)
Magnetite (Fe_3O_4)/LHRH metastatic tumors	10/?	Tail vein injection, 250 mg/kg NPs, 20 h	78 ± 24	4%	Prussian blue (luciferase for metastatic cells)	(18)
Magnetite (Fe_3O_4)/PEG (MW 5000)	10/~60	4 days, 37°C, 0.2 mg/ml NPs	113	5.9%	ICP	(16)
Magnetite/PEG–folic acid	44/~94	48 h, 37°C, unknown concentration	730	37.9%	ICP	(17)
Gold/citric acid	50	6 h, 37°C, 0.02 n*M* NPs	9000 NPs/cell	0.11%	ICP-AES, UV-Vis	(19)
Gold/folic acid– PEG (MW 1500)	10/~30	2 h, 37°C, ~5×10^{11} NPs/ml	10^{15} NPs/ml cell volume	0.05%	TEM on cryoslices	(32)

Notes. In converting between mass of iron and volume fraction, we use the published density for bulk iron oxide and assume a chemical formula of Fe_2O_3 except where noted. Using the formula Fe_3O_4 does not make a significant difference (~1%). For the gold nanoparticles, we also assume that the density of the nanoparticle cores is the same as that of bulk gold.

[a]For iron nanoparticles, loading is given in units of pg iron per cell.